DOI: 10.1021/ma9026564

Macromolecules
ARTICLE

Synthesis and Physical Properties of Reactive Amphiphilic Hydrogels Based on Poly(*p*-chloromethylstyrene) and Poly(ethylene glycol): Effects of Composition and Molecular Architecture

Caiping Lin[†] and Ivan Gitsov*[,†,‡]

[†]*Department of Chemistry and* [‡]*The Michael M. Szwarc Polymer Research Institute, State University of New York, College of Environmental Science and Forestry, Syracuse, New York 13210*

Received December 1, 2009; Revised Manuscript Received February 19, 2010

ABSTRACT: This paper describes the design, synthesis, and characterization of amphiphilic conetworks using linear or starlike poly(ethylene glycol), PEG, and linear or hyperbranched poly(*p*-chloromethylstyrene), PPCMSt. The initial synthetic strategy is based on the reaction between the hydroxyl end groups placed in the PEG and the primary and/or secondary alkyl chloride groups dispersed in the linear or hyperbranched component, respectively. It was found that the hybrid conetworks form in 55%−99% yields depending on the stoichiometric ratio of the two building blocks (19−0.5 g PEG per 1 g PPCMSt) and the type of polymer architecture. The dynamic swelling studies showed that the hydrogels absorb water quickly and reach equilibrium in 1−3 h. The architecture of starting polymer, PEG compositions, and temperature were the main factors affecting the equilibrium hydration of the cross-linked materials (700%−4200%). The observed high degree of swelling of these hydrogels in both water and organic solvents was attributed to the high network porosity, which was revealed by scanning electron microscopy (SEM) on freeze-dried specimens. The different states of water in the hydrated cross-linked matrices were measured by differential scanning calorimetry (DSC). The amounts of nonfreezing water, freezing bound water, and free water in the amphiphilic conetworks were dependent on their physicochemical structure.

Introduction

Amphiphilic hydrogels consisting of hydrophilic and hydrophobic segments are versatile materials, which are used extensively in both research and technology,[1−5] especially as devices for controlled release of pharmacological substances and biomaterials in tissue engineering. The key challenge in the design, preparation, and evaluation of amphiphilic networks is the identification and implementation of the most appropriate balance between hydrophobic and hydrophilic components, the cross-linking density, and the swelling ability that would be the most suitable for a particular application. It is believed that, by creating hydrophilic and hydrophobic microdomains throughout the cross-linked matrix (i.e., formation of a conetwork),[6] one could achieve a better regulation of hydrogel morphology and physical properties. In addition, these domains may serve as nanosinks or reservoirs for the loading and subsequent release of bioactive agents of different polarity.

Poly(ethylene glycol), PEG, is a nontoxic, water-soluble, biocompatible polymer, which is widely used in preparation of hydrogels.[7−12] These PEG-based networks can swell equally well in water and organic solvents, decrease the adsorption of proteins, and promote cell proliferation. Therefore, they are extensively evaluated in drug delivery and tissue engineering applications. Compared with the common linear polymer, star PEG has quasi-three-dimensional structure, in which several linear arms with reactive end groups emanate from a central core. In distinction to the linear derivative, star PEG has inherent branching, which could impart higher stability in the resulting network through a secondary cross-linking. These properties make it an excellent candidate as the hydrophilic component in amphiphilic hydrogel synthesis.

Dendritic macromolecules would also be the ideal candidates for cross-linking agents since they have highly branched structures and multiple reactive sites placed in the interior and at the periphery of the macromolecules.[13] Owing to this multifunctionality, bioactive molecules can be attached to cross-link junction fragments and physical properties such as swelling ability in selected solvents can be controlled by the chemical modification of the peripheral functional groups. Our previous studies revealed that the combination of PEG and hydrophobic poly(benzyl ether) dendrimers yields hydrogels with interesting properties and promising application potential.[14] Results show that most of the hyperbranched polymers also possess some of the unique properties exhibited by dendritic macromolecules, such as low viscosity, good solubility, and multifunctionality, but at much lower cost due to simple preparation procedures.[15] Few studies have been performed, however, where hyperbranched macromolecules were used as cross-linking agents.[16−18] For example, in an interesting series of investigations Wooley and co-workers have found that hydrogels containing fluorinated hyperbranched cross-links exhibit interesting antifouling properties.[16,17]

In this paper, we describe the synthesis and characterization of amphiphilic hydrogels, based on the chemical cross-linking of hyperbranched poly[(*p*-chloromethyl)styrene], H-PPCMSt, and poly(ethylene glycol), PEG. Our goal is to use the low cost hyperbranched polymer as the hydrophobic component and to investigate the influence of the balance of the two components on physical properties of amphiphilic hydrogels formed. The macromolecular architecture effect of the hydrophilic and hydrophobic components is traced by comparative studies with starlike PEG and the linear analogue of H-PPCMSt.

*To whom correspondence should be addressed.

 Published on Web 03/04/2010

Experimental Section

Materials. Linear poly(ethylene glycol), L-PEG (L-PEG 5K: M_n = 5000, M_w = 5400, M_w/M_n = 1.08; L-PEG 20K: M_n = 20 000, M_w = 22 000, M_w/M_n = 1.10) and four-arm star PEG, S-PEG (S-PEG 20K: M_n = 20 000, M_w = 23 000, M_w/M_n = 1.15, pentaerythritol core) from Polymer Source, Inc., were used in the experiments. Sodium hydride (NaH) (95%, dry powder), ethanol (95%), tetrahydrofuran (THF) (99.8%), and 2,2′-azobis(isobutyronitrile) (AIBN) were purchased from Aldrich. Chlorobenzene (99%) and *p*-chloromethylstyrene (90%) were obtained from Acros. Toluene (99.9%) from Fisher Scientific, dichloromethane (99.9%) from J.T. Baker, and chloroform (99.8%) from Mallinckrodt were used as received. *p*-Chloromethylstyrene was distilled under low pressure (0.4 mmHg, 45 °C), and AIBN was purified by recrystallization in ethanol. THF was dried over benzophenone sodium and distilled immediately before use. Toluene and chlorobenzene were dried with molecular sieves (4 Å, Fisher Scientific) prior to use.

Instrumentation and Analyses. Size-exclusion chromatography (SEC) analyses were conducted in THF (freshly distilled from KOH) on a line consisting of a Waters 510 pump, a Waters U6K universal injector, an Applied Biosystems 785A programmable UV−vis detector, and a Viscotek model 250 instrument for dual refractive index and viscometry detection. The separations were achieved at 40 °C across a set of three 5 μm PL gel columns (50 Å, 500 Å, and a mixed C) from Polymer Laboratories at eluent flow rate of 1 mL/min. The apparent molecular weights and polydispersities of the polymers were determined by calibration with 20 monodisperse polystyrene standards and OmniSEC software (Version 3.1) from Viscotek Corp.

Polymers and hydrogels were analyzed in a powder/particle form by a Magna 750 FT-IR spectrometer (Nicolet) using a MTEC 300 photoacoustic module from 500 to 4000 cm^{-1}.

^1H and ^{13}C NMR spectra were recorded in $CDCl_3$ at room temperature with a Bruker Avance 300 instrument (^1H: 300 MHz).

Differential scanning calorimetry (DSC) was conducted on TA Instrument 2920 modulated differential scanning calorimeter under nitrogen applying a heating/cooling/heating cycle between −60 and +120 °C with a scanning rate of 5 °C/min. The average sample size was 8 ± 2 mg. The temperature of the melting/crystallization transitions was determined at the intersection of the two tangents drawn at the two slopes of the transition peak. The measurement of free and bound water in the swollen hydrogels was investigated using previously described procedure.[19] The water content of the sample after the initial soaking was adjusted by allowing water to evaporate from the sample in a desiccator containing silica gel at room temperature. The samples were then hermetically sealed in aluminum pans, cooled to −70 °C, and then heated to 40 °C, at heating rate of 2−5 °C/min under 110 mL/min nitrogen gas flow.

The specific water content fraction (f_{water}) of hydrogels was expressed by the following equation:

$$f_{water} = (W_{wet} - W_{dry})/W_{wet} \times 100\%$$

where W_{wet} and W_{dry} are the weights of the sample in the swollen and dry states, respectively. The total water in the swollen hydrogels was determined with a thermogravimetric analyzer TGA Q500 (TA Instruments) by heating of samples under a nitrogen atmosphere from room temperature to 300 °C, at a heating rate of 10 °C/min.

Scanning electron micrographs (SEM) images were obtained by using a JEOL-5800-LV SEM instrument with acceleration voltage 5−10 kV. The swollen hydrogel samples were immersed in water for 48 h and then quickly frozen with liquid nitrogen. The frozen hydrogels were subjected to cryo-fracturing followed by lyophilization. The dry samples were sputter-coated with palladium and gold for SEM examination.

Synthesis. *Synthesis of Linear Poly(p-chloromethylstyrene), L-PPCMSt, by Classical Free Radical Polymerization. p*-Chloromethylstyrene (5 mmol) was mixed with AIBN at monomer to initiator ratios ([M]/[I]) in the range of 6.25−100, and then chlorobenzene or toluene (1.8 mL) was added. The mixed solution was stirred in a nitrogen atmosphere in an oil bath at 75−80 °C (chlorobenzene) or 60 °C (toluene). The viscosity of the solution increased as polymerization proceeded, and the color of solution changed to a light yellow. After 24 h the polymer was precipitated into methanol to form a white powder and then filtered. The precipitate was dissolved in THF and reprecipitated into methanol. The process was repeated twice, and the final product was then dried under vacuum at room temperature (yield 72%−95%). These polymers had molecular weights averaging between 2.7×10^3 and 2.04×10^4 Da as estimated by SEC. They were further characterized by FT-IR and ^1H NMR. FT-IR: 3023.9, 2927.5, 2850.3, 1700.9, 1608.4, 1511.9, 1484.9, 1446.4, 1423.2, 1265.1, 836.9, 798.4, 709.7, 674.9, 609.4 cm^{-1}. ^1H NMR ($CDCl_3$): δ 1.46 (CH_2−CHAr), 1.73 (CH_2−CHAr), 4.51 (CH_2Cl), 6.50 and 7.06 (ArH).

Synthesis of Hyperbranched Poly(p-chloromethylstyrene), H-PPCMSt, by Metal-Mediated Controlled Radical Polymerization. Hyperbranched PPCMSt was synthesized according to previously published procedure.[20] The preparation was conducted as follows: 2,2′-bipyridyl (8.4 mmol) and CuCl (4.2 mmol) were added to a cylindrical reaction vessel, followed by addition of chlorobenzene (8.0 mL) and *p*-(chloromethyl)-styrene (21 mmol). Then the reaction mixture was flushed with nitrogen and placed in an oil bath (115 °C). After ∼40 min, a green solid precipitated. Polymerization went on for 4 h. Then the reaction vessel was moved out of the oil bath and allowed to cool down for 30 min. THF (50 mL) was added to the reaction mixture, which was then stirred at room temperature overnight to complete the dissolution of the polymer and to allow for catalyst oxidization. The solution was filtered through alumina to remove the insoluble salts. The resulting clear brown solution was concentrated and precipitated into methanol. The off-white powder precipitate was dried under vacuum. The polymers were obtained with weight-average molecular weights between 2.4×10^3 and 4.5×10^4 Da by SEC and the ratios of secondary (4.75 ppm) to primary benzyl chloride (4.5 ppm) groups about 0.18−0.33 at monomer to catalyst ratios in the range of 5−20. FT-IR: 3023.5, 2930.6, 2856.1, 1699.3, 1605.5, 1511.6, 1487.8, 1445.1, 1423.7, 1266.4, 1165.0, 1017.6, 899.6, 828.6, 795.9, 706.5, 677.0, 631.9 cm^{-1}. ^1H NMR ($CDCl_3$): δ 1.55 (CH_2−CHAr), 1.90 (CH_2−CHAr), 4.50 (CH_2Cl), 4.75 (CHCl), and 6.50−7.41 (ArH).

General Procedure for the Synthesis of Amphiphilic Hydrogels. Star or linear PEG and linear PPCMSt or hyperbranched PPCMSt were mixed in different ratios (19−0.5 g PEG/1 g PPCMSt) in a pear-shaped flask. Dried THF (1 mL, 2.5 or 5.0 mL) was used as the solvent to dissolve both reagents. NaH was added to the stirred solution at room temperature to catalyze the reaction. As a result, the color of the reaction mixture changed from a clear and colorless to light yellow with precipitate forming over several hours, depending on the reagents and the initial reagent concentration. After 24 h, ethanol was added to stop the reaction and consume the excess NaH. The solution was centrifuged, and the solid residue was washed consecutively with ethanol and chloroform to remove the unreacted residual PEG and PPCMSt fragments. Distilled water was used to wash out the side product, NaCl. The hydrogel samples were then quickly frozen in liquid nitrogen and dried by lyophilization for 24−48 h. Yield (10%−90%) was calculated as the ratios of the mass of the products to the total amounts of original two building blocks. The formal designations of the cross-linked products used throughout the discussion are as follows: S(*X*)L for gels derived from star PEG and linear PPCMSt; S(*X*)H for products obtained from star PEG and hyperbranched-PPCMSt; L(*Y*)L for conetworks formed by linear-PEG and linear-PPCMSt; and

Scheme 1. Synthesis of Hydrogels from Star PEG and Hyperbranched or Linear PPCMSt

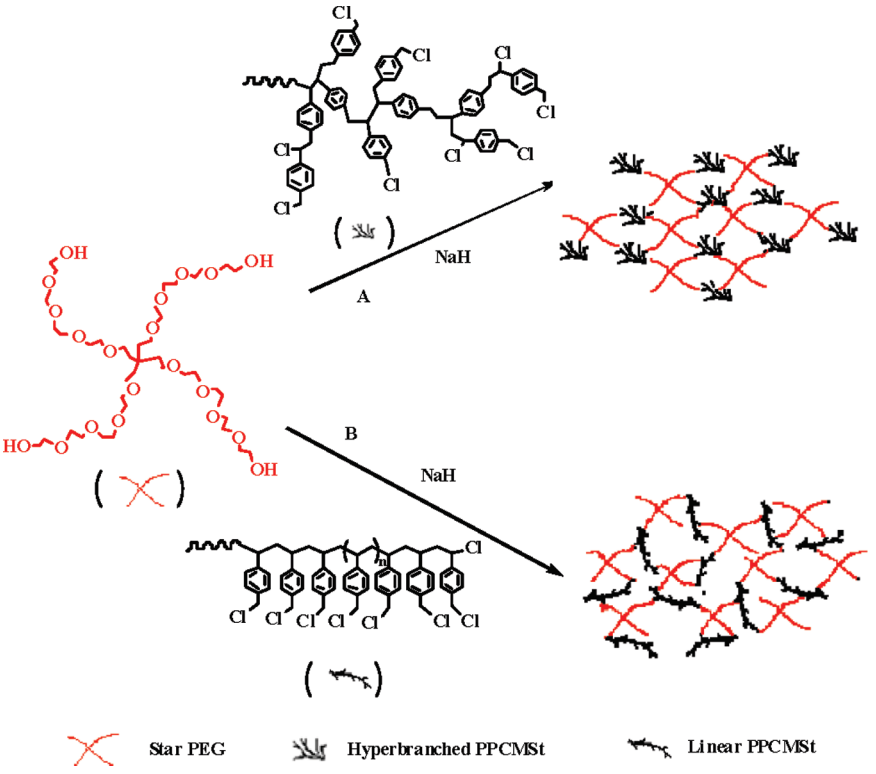

Scheme 2. Synthesis of Hydrogels from Linear PEG and Hyperbranched or Linear PPCMSt

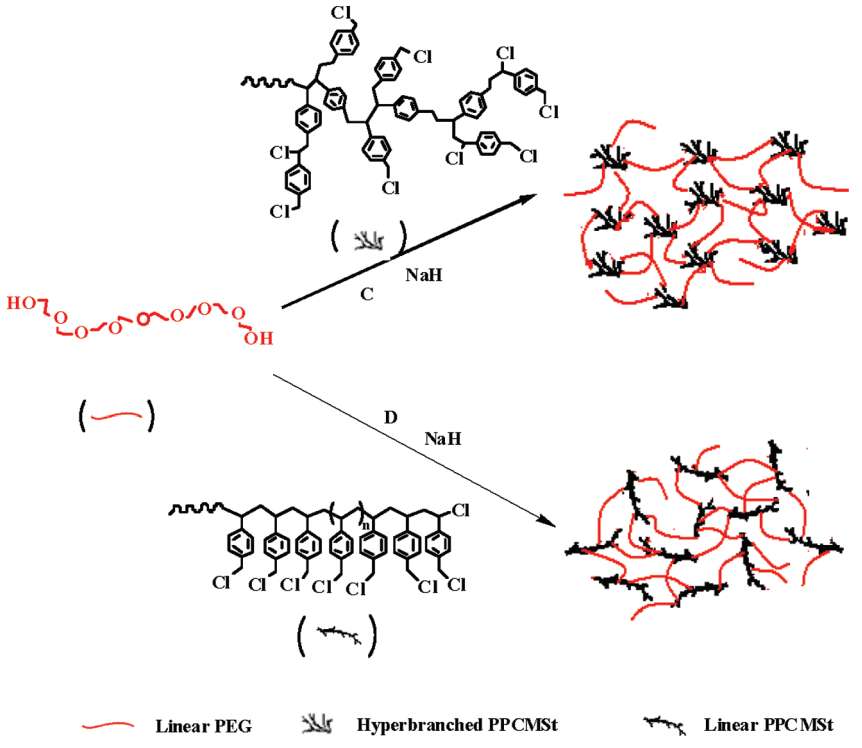

L(*Y*)H for gels consisting of linear PEG and hyperbranched PPCMSt (X = 20, Y = 5 or 20). DSC, FT-IR, and swelling measurements were conducted on representative samples of the purified hydrogels.

Swelling Experiments. Before the swelling measurements were carried out, all hydrogels were extracted with ethanol and chloroform and multiple portions of DI water. They were then dried in the lyophilizer. The swelling behavior of networks with varying PEG and PPCMSt content was investigated as a function of time and temperature.

Kinetics of Swelling. Dynamic swelling studies were also conducted to elucidate the mechanism of water diffusion into the polymer networks based on PPCMSt and PEG as determined by the dynamic portion of the gravimetric curve. The kinetics of swelling was measured as follows: ~15 mg of hydrogels was measured and placed in a vial containing 20 mL of DI

water. The vial was placed into a water bath equilibrated at specific temperature (37 ± 0.2 °C). The specimens were periodically weighted through the experiment. The water uptake, M_t, was followed as a function of time until equilibrium was attained. It was calculated from the average of the final weights using the formula

$$M_t = (W_{wet} - W_{dry})/W_{dry} \times 100\%$$

Swelling Ratio. The weight swelling ratio was calculated as the ratio of the weight of the swollen hydrogels to the weight of the original dry gel according to the following procedure. The weight of the dry samples was recorded before they were immersed in a large excess of the corresponding solvent (DI water, toluene, THF, or CH_2Cl_2) at room temperature. After at least 24 h the specimens were weighted again after the solvent droplets on the surface of the samples were carefully blotted with lint-free paper. The weight swelling ratio (q) was calculated as follows:

$$q = W_{wet}/W_{dry}$$

where W_{wet} and W_{dry} are the weights of swollen and dry sample, respectively.

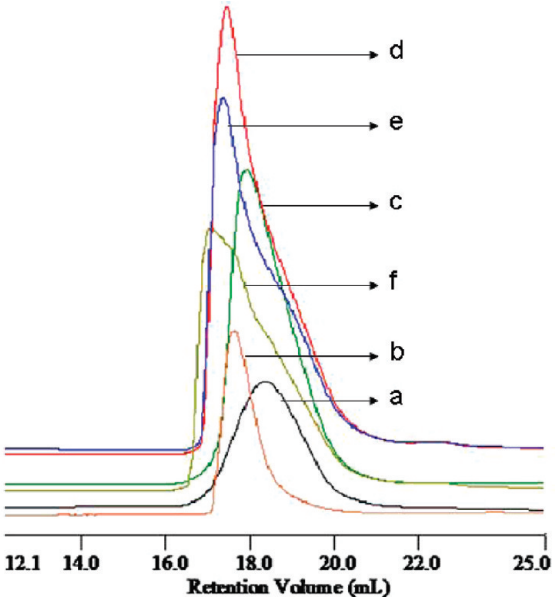

Figure 1. SEC with dRI detection of (a) linear PPCMSt (M_n = 5200, M_w = 7100); (b) S-PEG 20K and reaction mixtures at (c) 0, (d) 1, (e) 2, and (f) 5 h. Solvent: THF (5.0 mL).

Results and Discussion

Hydrogel Syntheses. The chemical cross-linking used for the formation of amphiphilic hydrogels is achieved by surface-to-surface connection of star PEG (S-PEG) with hydroxyl end groups to hyperbranched globules (Scheme 1, path A) or linear chains (Scheme 1, path B), which have primary and secondary methyl chloride moieties. The networks formed have two types of cross-link junctions incorporated—a small hydrophilic moiety in the S-PEG and large hydrophobic one in the hyperbranched or linear PPCMSt. This double cross-link density would probably impart higher rigidity and mechanical strength in the hydrogels but would inevitably decrease their swelling abilities. For comparison purposes, linear PEG with different chain length is also used to synthesize amphiphilic hydrogels (Scheme 2, paths C and D). The networks produced by this combination contain only one type of cross-link junction—the hydrophobic linear or hyperbranched PPCMSt and would have higher degree of swelling and flexibility. Both procedures yield networks, which swell uniformly in water.

SEC is used to monitor the reaction progress. Starting reagent peaks of linear PPCMSt and S-PEG (Figure 1, a and b, respectively) decrease after 1 h, and a new peak of higher molecular weight is formed (Figure 1d). It should be mentioned that in a relatively diluted regime the reaction products remain soluble due most probably to very loose and/or limited cross-linking. In contrast, at high reagent

Table 1. Yields and Weight Swelling Ratios of Hydrogels Series S20H Formed by Reaction of Star PEG (Four Arms, M_w = 22 000) and Hyperbranched PPCMSt (M_n = 5000, M_w = 16 500)

entry	weight feeding ratio S-PEG20K:H-PPCMSt	PEG (wt %)	yield (%)	weight swelling ratios			
				DI water	toluene	THF	CH_2Cl_2
1	19:1	95	55	35.8 ± 0.5	26.2 ± 1.0	26.4 ± 0.5	65.5 ± 0.4
2	9:1	90	84	34.2 ± 1.0	22.3 ± 0.3	24.3 ± 0.5	65.2 ± 1.3
3	6:1	85	87	33.9 ± 0.8	23.2 ± 0.1	26.1 ± 0.1	62.9 ± 0.3
4	4:1	80	92	33.0 ± 0.5	22.6 ± 0.1	26.1 ± 0.6	60.2 ± 1.8
5	3:1	75	94	26.5 ± 0.6	23.2 ± 0.6	23.0 ± 0.9	54.0 ± 0.2
6	2:1	67	91	23.9 ± 0.2	26.5 ± 0.9	26.3 ± 1.6	50.3 ± 1.7
7	1:1	50	90	15.2 ± 0.7	22.2 ± 0.1	19.7 ± 0.7	33.7 ± 1.4
8	1:2	33	64	11.7 ± 0.3	22.7 ± 0.1	23.3 ± 0.4	38.2 ± 0.4

Table 2. Yields and Weight Swelling Ratios of Hydrogels Series S20L Formed by Reaction of Star-PEG (Four Arms, M_w = 22 000) and Linear PPCMSt (M_n = 10 000, M_w = 16 800)

entry	weight feeding ratio S-PEG20K:L-PPCMSt	PEG (wt %)	yield (%)	weight swelling ratios			
				DI water	toluene	THF	CH_2Cl_2
1	19:1	95	84	30.4 ± 0.5	20.0 ± 1.4	21.3 ± 0.5	63.9 ± 0.8
2	9:1	90	93	29.0 ± 0.8	26.6 ± 0.4	24.0 ± 0.3	62.9 ± 0.3
3	6:1	85	93	23.7 ± 0.2	27.5 ± 0.3	24.1 ± 0.3	56.6 ± 0.6
4	4:1	80	96	22.9 ± 0.3	27.5 ± 0.3	24.8 ± 0.3	53.9 ± 0.4
5	3:1	75	95	21.3 ± 0.2	28.0 ± 0.5	24.0 ± 0.6	51.2 ± 0.3
6	2:1	67	95	19.1 ± 0.3	30.9 ± 0.3	22.9 ± 0.6	50.2 ± 0.7
7	1:1	50	96	17.8 ± 0.5	27.5 ± 1.4	23.4 ± 1.2	46.8 ± 1.4
8	1:2	33	79	12.1 ± 0.5	17.7 ± 0.3	18.2 ± 0.1	36.1 ± 0.4

Table 3. Yields and Weight Swelling Ratios of Hydrogels Series L20H Formed by Reaction of Linear PEG (M_w = 23 000) and Hyperbranched PPCMSt (M_w = 16 500)

entry	weight feeding ratio L-PEG20K:H-PPCMSt	PEG (wt %)	yield (%)	weight swelling ratios			
				DI water	toluene	THF	CH_2Cl_2
1	19:1	95	79	43.7 ± 1.5	15.6 ± 0.5	24.3 ± 0.5	71.2 ± 0.8
2	9:1	90	91	42.7 ± 0.5	15.5 ± 0.7	23.3 ± 0.5	68.6 ± 0.3
3	6:1	85	91	42.1 ± 0.3	17.0 ± 0.5	24.0 ± 0.1	69.5 ± 1.4
4	4:1	80	92	35.0 ± 1.4	21.0 ± 1.2	23.7 ± 0.4	59.4 ± 0.4
5	3:1	75	93	29.9 ± 0.2	27.0 ± 0.3	26.3 ± 0.6	59.0 ± 1.7
6	2:1	67	91	21.8 ± 0.4	28.5 ± 0.2	27.3 ± 0.7	49.3 ± 1.3
7	1:1	50	92	17.8 ± 0.2	27.1 ± 0.9	26.3 ± 0.7	43.4 ± 0.7
8	1:2	33	90	16.3 ± 0.3	20.7 ± 0.2	23.2 ± 0.1	39.7 ± 0.3

Table 4. Yields and Weight Swelling Ratios of Hydrogels Series L20L Formed by Reaction of Linear PEG (M_w = 23 000) and Linear PPCMSt (M_w = 16 800)

entry	weight feeding ratio L-PEG20K:L-PPCMSt	PEG (wt %)	yield (%)	weight swelling ratios			
				DI water	toluene	THF	CH_2Cl_2
1	19:1	95	84	37.1 ± 0.4	24.2 ± 0.3	24.8 ± 0.1	65.6 ± 0.1
2	9:1	90	93	32.6 ± 0.2	23.8 ± 1.0	24.3 ± 1.3	64.6 ± 2.2
3	6:1	85	98	22.8 ± 0.3	20.1 ± 0.2	18.7 ± 0.1	46.7 ± 0.9
4	4:1	80	98	19.9 ± 0.2	20.1 ± 0.3	16.9 ± 0.8	45.2 ± 0.7
5	3:1	75	99	18.4 ± 1.2	21.5 ± 0.4	21.2 ± 0.4	45.8 ± 0.5
6	2:1	67	98	18.4 ± 0.3	20.2 ± 0.4	20.0 ± 0.4	43.2 ± 0.3
7	1:1	50	93	17.1 ± 0.3	21.5 ± 1.3	21.6 ± 0.8	43.0 ± 2.0
8	1:2	33	78	16.2 ± 0.2	15.7 ± 0.1	16.9 ± 0.2	33.4 ± 0.3

Table 5. Yields and Weight Swelling Ratios of Hydrogels Series L5H Formed by Reaction of Linear PEG (M_w = 5400) and Hyperbranched PPCMSt (M_w = 16 500)

entry	weight feeding ratio L-PEG5K:H-PPCMSt	PEG (wt %)	yield (%)	weight swelling ratios			
				DI water	toluene	THF	CH_2Cl_2
1	6:1	85	66	24.1 ± 0.3	16.8 ± 0.1	21.0 ± 0.7	45.8 ± 1.2
2	4:1	80	88	19.2 ± 0.2	16.3 ± 0.1	17.4 ± 0.1	39.0 ± 0.3
3	2:1	67	91	16.6 ± 0.4	17.0 ± 0.1	17.5 ± 0.1	37.2 ± 0.7
4	1:1	50	91	16.0 ± 0.4	19.3 ± 0.7	18.4 ± 0.1	36.6 ± 1.1
5	1:2	33	91	10.4 ± 0.2	16.0 ± 0.1	18.2 ± 0.1	30.4 ± 0.3

Table 6. Yields and Weight Swelling Ratios of Hydrogels Series L5L Formed by Reaction of Linear PEG (M_w = 5400) and Linear PPCMSt (M_w = 16 800)

entry	weight feed ratio L-PEG5K:L-PPCMSt	PEG (wt %)	yield (%)	weight swelling ratios			
				DI water	toluene	THF	CH_2Cl_2
1	6:1	85	90	15.3 ± 0.1	14.7 ± 0.1	14.4 ± 0.3	36.8 ± 0.3
2	4:1	80	94	14.7 ± 0.1	14.8 ± 0.1	15.6 ± 0.1	37.7 ± 0.1
3	2:1	67	98	10.0 ± 0.1	14.6 ± 0.1	14.0 ± 0.8	34.1 ± 0.9
4	1:1	50	99	9.6 ± 0.1	19.3 ± 0.1	18.5 ± 0.4	41.0 ± 0.3
5	1:2	33	97	7.7 ± 0.1	23.6 ± 0.1	21.6 ± 0.1	41.7 ± 0.3

concentration (THF = 2.5 and 1.0 mL), the viscosity of the reaction mixture increases rapidly and further SEC analysis is prevented by the gelation of the system.

The composition of the gels could be controlled directly by altering the weight feeding ratio of two components in the initial reaction mixture. We prepared hydrogels with 33 to 95 wt % of PEG (weight feed ratio of PEG to PPCMSt is 2/1 to 19/1, respectively). Tables 1−6 give the PEG to PPCMSt feed ratios, yields, and swelling ratio data of the hydrogels in different solvents. The feed ratio of PEG to PPCMSt from 1 to 6 is the optimal proportion, at which high yields (≥90%) for both linear- and S-PEG can be achieved, while the cross-linking efficiency is rather low when the reagent weight feed ratio is outside of this range.

Under identical reaction conditions linear PPCMSt affords hydrogels with higher yields than the hyperbranched analogue. The probable reason is the difference in the macromolecular architecture, the number of spatially available functional groups, and their reactivity. The molecular shape of the hyperbranched block is more spherical, and a portion of reactive functional groups is hidden inside this globule. Moreover, H-PPCMSt contains 21.8% of the less reactive secondary methyl chloride, compared with L-PPCMSt, where the more reactive primary methyl chloride groups comprise 100% of the cross-linking functionalities. Therefore, the hydrogels made from hyperbranched PPCMSt would have lower average cross-link density as evidenced by their higher swelling ratios measured in solvents of different polarity (Tables 1−4). The addition of a second cross-link modality (star-PEG) induces the same effect—the resulting networks are more rigid (Tables 1 and 2).

The molecular weight of PPCMSt and solvent amount in the reaction mixture also affect the yields of the hydrogel

Table 7. Yields of Hydrogels Formed by Reaction of PEG and Linear PPCMSt

entry	weight feed ratio PEG:L-PPCMSt	type of PEG (80 wt % PEG)	M_n of L-PPCMSt	M_w of L-PPCMSt	yield (%)
1	4:1	star PEG 20K	2500	3560	68
2	4:1	star PEG 20K	5200	7100	90
3	4:1	star PEG 20K	11000	16800	96
4	4:1	linear PEG 20K	2500	3560	25
5	4:1	linear PEG 20K	5200	7100	95
6	4:1	linear PEG 20K	11000	16800	98

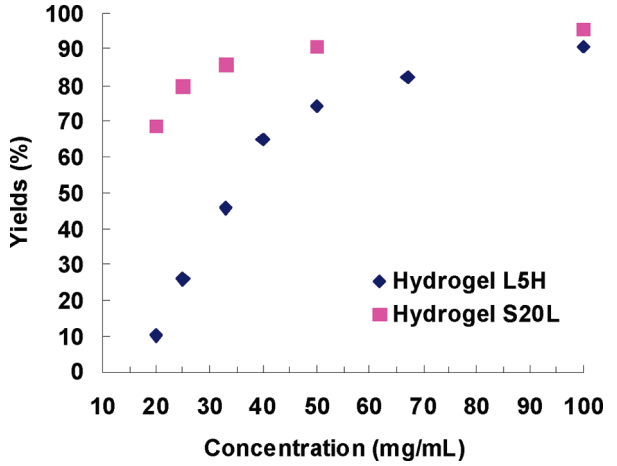

Figure 2. Hydrogels (series L5H 50 wt % PEG and S20L 80 wt % PEG) yields at different solvent volume (THF 1−5 mL, 100−20 mg/mL).

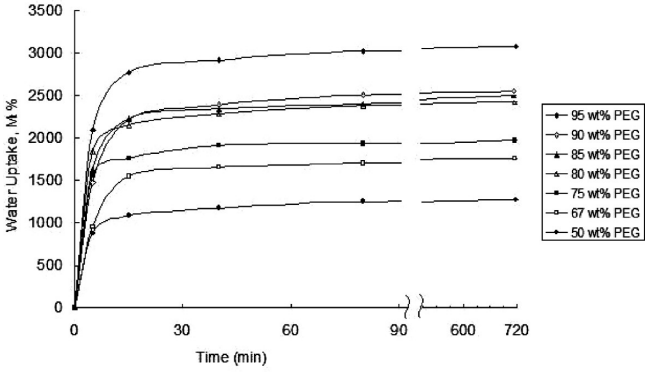

Figure 3. Percentage mass swelling as a function of time for the hydrogel series S20H (Table 1).

formed. A higher molecular weight PPCMSt affords more hydrogel than the one with low molecular weight (Table 7) due to the larger number of cross-linking moieties. Figure 2 shows yields of hydrogels series of S20L and L5H prepared with different reagents concentration (20−100 mg/mL), but using the same weight feeding ratio. It is evident that the yields of both hydrogels increase with concentration regardless of the starting polymer architectures. The hydrogels prepared at the higher concentrations are more resistant to breakage, whereas those prepared at low concentration are more fragile. These observations confirm the common trend encountered in the typical network synthesis that the cross-link density normally increases with the concentration of the reaction mixture.

Characterization of Hydrogels Prepared from PEG and Linear or Hyperbranched PPCMSt. The application potential of hydrogels depends on their hydrophilicity and their behavior in aqueous media. Therefore, the investigation of

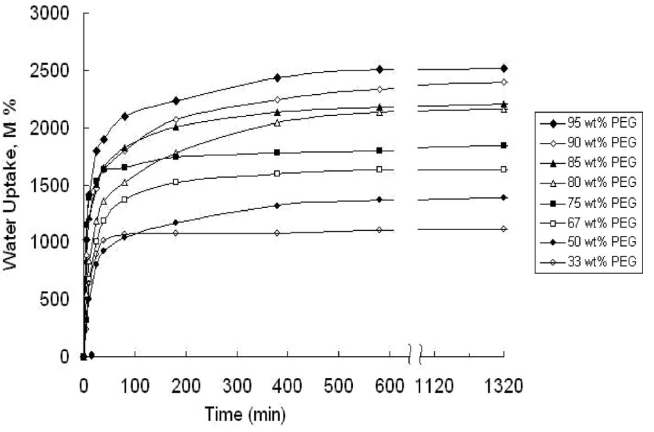

Figure 4. Percentage mass swelling as a function of time for the hydrogel series S20L (Table 2).

the structural changes and dependencies in this medium is of particular importance.

Dynamic Swelling Studies. The dynamic swelling experiments are performed to elucidate the mechanism of water diffusion into hydrogels as determined by the water uptake of hydrogels. Figures 3 and 4 show the dynamic water swelling plots of hydrogels built of star PEG 20K and hyperbranched or linear PPCMSt at different composition ratios (Tables 1 and 2, entries 1−8). All curves show a rapid initial absorption of water within the first 10−20 min, followed by decreased rate stage, and finally the systems approach equilibrium after 0.5−2 h (Figures 3 and 4). Although the same series of the hydrogels showed similarities in the swelling rate patterns, there was a significant difference in the equilibrium swelling ratio. The equilibrium percentage of water uptake for hydrogel S20H increases from 1329 to 3145 as the PEG content increased from 50% to 95%, while the uptake for hydrogel S20L increases from 1112 to 2591 at the same range. The hydrogels made from linear PEG 20K and 5K with hyperbranched or linear PPCMSt showed similar dynamic swelling behavior as hydrogels from star PEG 20K.

The swelling profile of the hydrogels is sensitive not only to their composition but also to the macromolecular architecture of both constituents. Comparing the data in Figures 3 and 4, it is obvious that the hydrogels made of hyperbranched PPCMSt are swelling faster than the hydrogels made of the linear analogue. Also, the hydrogels made by linear PPCMSt have a lower equilibrium weight swelling ratio compared with the hyperbranched networks. Very similar trends have been observed for those hydrogels made of linear PEG 20K or 5K with the same hyperbranched or linear PPCMSt. As expected, the more globular hyperbranched polymers have more concentrated cross-link populations in a smaller volume than their linear counterparts of similar molecular weight. Thus, at the same reaction conditions, the hydrogel synthesized with H-PPCMSt would have a bigger mesh size than the hydrogel made with L-PPCMSt

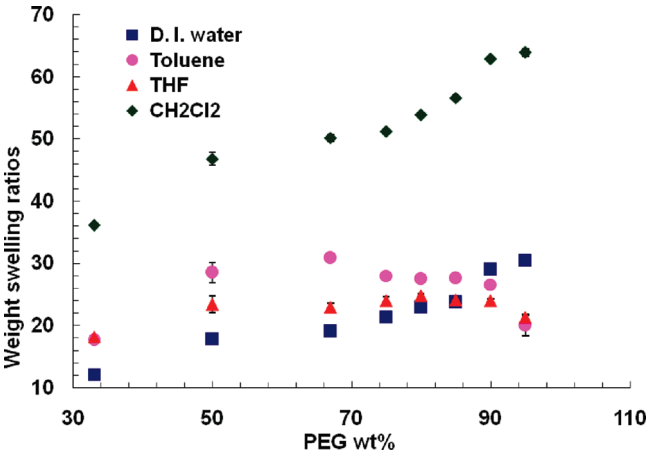

Figure 5. Weight swelling ratio of hydrogel series S20L in four solvents of different polarity.

Scheme 3. Morphology of Hydrogel Made from Hyperbranched (a) or Linear PPCMSt (b)

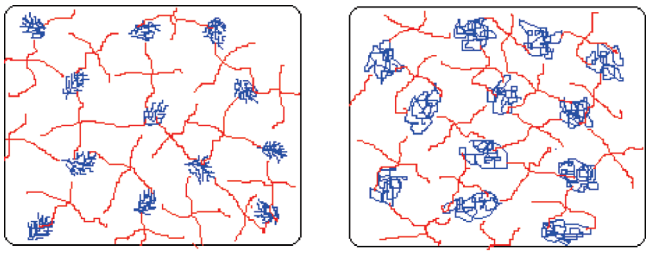

(Scheme 3). The randomly distributed big pores facilitate the faster swelling of the networks and the increase in the absorbed water at equilibrium. These assumptions are further supported by SEM photographs, which will be discussed later.

Swelling Ratio. In general, the major factors that affect swelling behavior of amphiphilic hydrogels are the composition and cross-linking density. The equilibrium swelling of hydrogels S20L in deionized water and in three organic solvents measured as a function of the content of PEG is shown in Tables 1−7 and Figure 5. It can be seen that as the feed ratio of PEG to PPCMSt decreases, the hydrogels become more hydrophobic and have lower weight swelling ratio in DI water. For organic solvents (THF, CH_2Cl_2, or toluene), where both constituents have relatively good solubility, the trend for the weight swelling ratio is not so obvious. It is seen that at low PEG content the degrees of swelling in all three organic solvents are rather close, reflecting the similarities in their χ parameters.[21] Obviously, the swelling behavior in these media also depends on additional factors besides the two mentioned above: the architecture (i.e., the intrinsic rigidity of the building blocks) and the morphology of hydrogels.

It is found that at very high PEG content (> 90 wt %) the equilibrium water absorbency of the hydrogel series, made by linear PEG 20K, is much higher than the series of star-PEG 20K, which in turn is much higher than those from linear PEG 5K. As the PEG content decreases, the gap in equilibrium swelling ratio for those hydrogels decreases or disappears (Figure 6). For samples with the same PPSMSt and PEG composition, the equilibrium swelling ratio would be affected only by the cross-linking density and the interlink distance (length). For the three types of PEG, investigated in

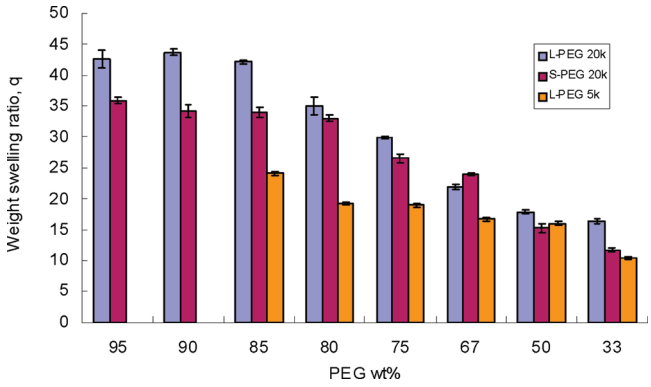

Figure 6. Weight swelling ratio of hydrogels from three types of PEG and hyperbranched PPCMSt in DI water.

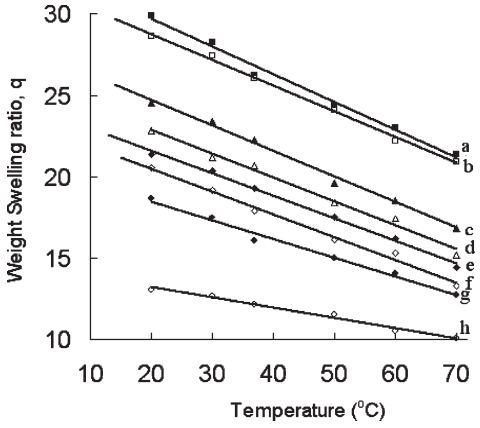

Figure 7. Temperature effects on the swelling behavior of hydrogels series S20L (a: 95 wt % PEG, slope = −0.169; b: 90 wt % PEG, slope = −0.158; c: 85 wt % PEG, slope = −0.157; d: 80 wt % PEG, slope = −0.148; e: 75 wt % PEG, slope = −0.139; f: 67 wt % PEG, slope = −0.141; g: 50 wt % PEG, slope = −0.116; h: 33 wt % PEG, slope = −0.063).

this study, in the high PEG wt % area, linear PEG 20K has the highest ratio of methyl chloride to hydroxyl equivalent and would lead to a network with the lowest degree of cross-linking density and the largest interjunction distance, while the incorporation of linear PEG 5K would result in higher cross-linking density and the shortest interjunction length as evidenced by its lower swelling ratio. The star PEG 20K could be regarded as a superposition of two PEG chains with molecular weight of 10 kDa, which is reflected in the medium swelling ratio observed. The influence of the PEG size would diminish with the decrease of its content (the increased fraction of the hydrophobic component should dominate the swelling behavior in water), and the differences in swelling are smaller (Figure 6).

The temperature also affects the swelling behavior of hydrogels. The data in Figure 7 show a linear dependence between the sample swelling mass of hydrogels S20L and the temperature. In most cases the gels have the highest swelling ratios at low temperature because the PEG exhibits a lower critical solution temperature (LCST).[22] The apparent absence of abrupt phase transition (separation) in the temperature interval studied (the expected LCST should occur between 30 and 50 °C[22b]) could be attributed to the chemical and architectural composition of the cross-linked matrix. Hydrogels containing high weight percentages of PEG change more notably upon temperature change, as evidenced by the high slope in the corresponding fitting trend lines. As the PEG content goes down, the difference

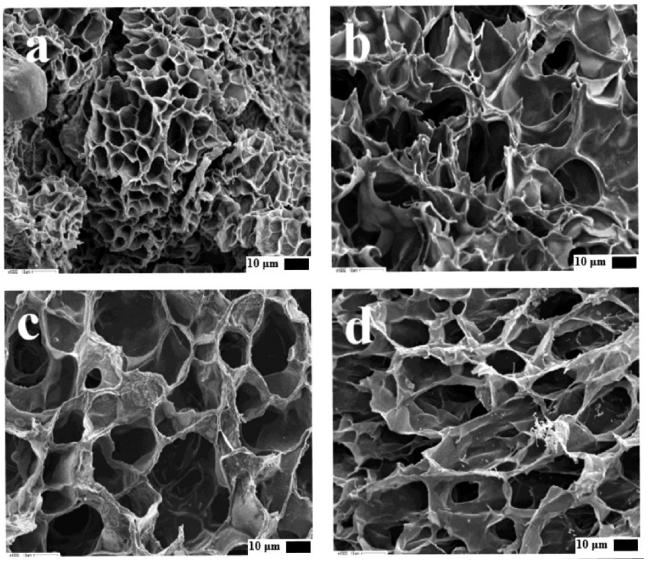

Figure 8. SEM images of hydrogels from linear PEG 20K and linear PPCMSt (a: 33; b: 50; c: 80; d: 95 wt % of PEG). Magnification 1000× (scale bar: 10 μm).

of swelling ratio for the different temperatures decreases (Figure 7a,h).

Morphology. The pore size and pore size distribution affect some of the physical properties of many hydrogels and frame their application areas.[23−25] Electron microscopy is a particularly useful analytical technique, which provides insight into the gel structure with various levels of resolution. The high degree of swelling of the hydrogels suggests that upon lyophilization highly macroporous spongelike scaffolds could be produced.

Figure 8 shows the SEM photographs of the hydrogel microstructures for series L20L, formed with linear PPCMSt and linear PEG 20K (33, 50, 80, and 90 wt % of PEG). The hydrogel with 33 wt % of PEG has a spongelike macroporous organization with pore diameter 4−8 μm and with a relatively uniform pore size distribution. It is observed that the pore size becomes bigger as the PEG content increases. When the wt % of PEG reaches 95%, more aggregated and open-cell pores are observed inside the network matrix. The morphology observed by SEM might offer insights into the physical properties and behavior of the hydrogels. Macropores are effective solvent reservoirs, and the diffusion rate and permeability of small compounds through hydrogels with open-cell (pores within pore) structure are significantly higher. The hydrogels with higher PEG content have large and open-cell pores and therefore exhibit rapid water adsorption and higher equilibrium swelling. Thus, the SEM observations support the experimental swelling data in the previous section.

The structures of hydrogels prepared by linear or hyperbranched PPCMSt with the same PEG 20K (Figure 9e,f or Figure 9g,h) are different. It is evident that a more open-cell (pores within pore) organization is achieved with H-PPCMSt (Figure 9f,h), which correlates nicely with their faster swelling as described in the previous section. There is also a difference in the microstructure of the hydrogels from the linear PEG and star-PEG with the same PPCMSt (Figure 9e,g or Figure 9f,h). The average pore size in the hydrogel, made from S-PEG 20K, is 4−5 μm (Figure 9g), while the pores in the hydrogel from L-PEG 20K measure 8−9 μm. Star-PEG imparts a double cross-linking in the networks formed and leads to a smaller pore size morphology. In particular, the hydrogel made from S-PEG and H-PPCMSt shows a large population of interconnected pores.

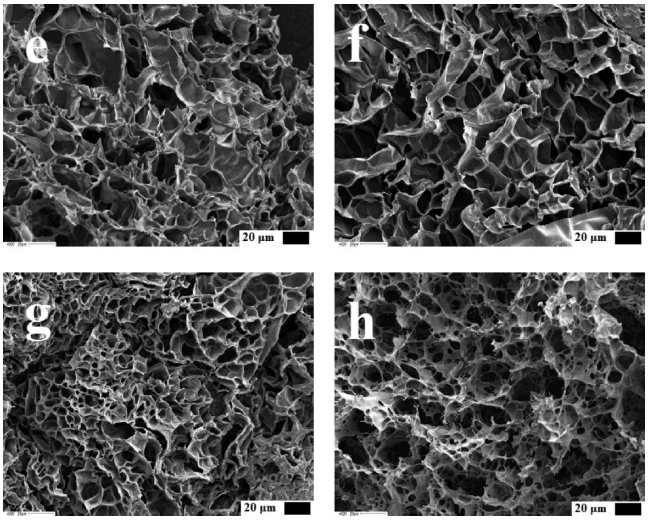

Figure 9. SEM images of hydrogels from linear PPCMSt (e: 50 wt % of L-PEG 20K; g: 50 wt % of S-PEG 20K) or hyperbranched PPCMSt (f: 50 wt % of L-PEG 20K; h: 50 wt % of S-PEG 20K). Magnification 500× (scale bar: 20 μm).

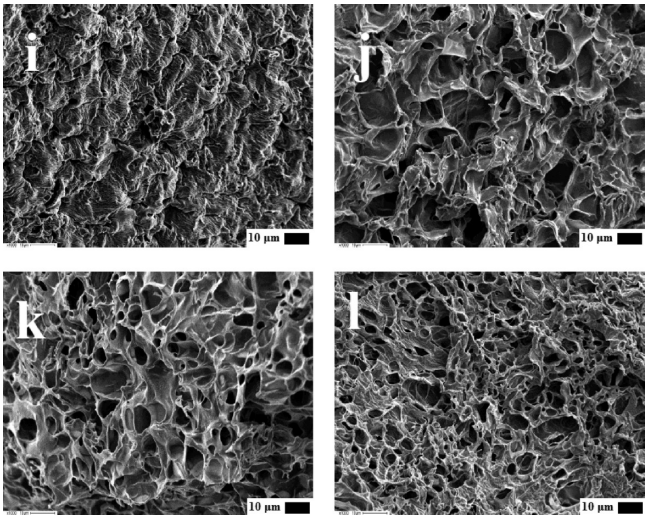

Figure 10. SEM images of hydrogels from linear PEG 5K and linear PPCMSt (i, 33; j, 50; k, 67; l, 80 wt % of PEG). Magnification 1000× (scale bar: 10 μm).

The morphology of hydrogels made from linear PEG 5K is notably different from those made from PEG 20K. At low PEG content, no pores could be detected (Figure 10i,j). When the wt % of PEG increases to 67, small pores (about 4 μm) start to appear, and no open-cell structure can be seen in all hydrogel samples (Figure 10k,l). This result also correlates well with the previously discussed swelling study, where it was found that the L-PEG 5K hydrogels have a much lower swelling ratio (S = 6.7−14.3) than the L-PEG 20K hydrogel (S = 11.4−36.1).

One of the goals of this study is to compare the previously reported[14a,c] amphiphilic hydrogels produced with third generation, [G-3], poly(benzyl ether) dendrimers and networks of hyperbranched hydrophobic fragments with somewhat analogous structure and molecular weight characteristics. The evaluation is performed with two families of cross-linked materials containing 80−90 wt % of L-PEG as the hydrophilic component. The swelling studies in water reveal that

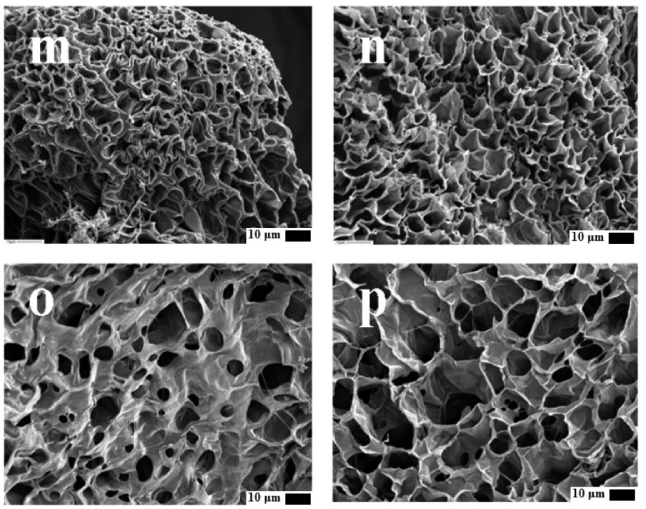

Figure 11. SEM images of hydrogels from linear PEG 3.4K and [G-3] dendrimer (m, 81 wt %; n, 89 wt % of PEG) and linear PEG 5K and hyperbranched PPCMSt (o, 80 wt %; p, 90 wt % of PEG). Magnification 1000× (scale bar: 10 μm).

the dendritic hydrogels expand (absorb) significantly less than the hyperbranched ones: $S = 3-7$ vs $S = 18-23$ (ref 14a,c and Table 5). Similar trends are observed for organic solvents (THF, toluene, and dichloromethane) as well. The micrographs of the two gel series are shown in Figure 11. Both networks have porous structure, but the hyperbranched hydrogel contains interconnected pores with larger diameters (Figure 11 o,p). This would allow water to diffuse more easily within the gel matrix during the swelling process, and more solvent would be entrapped at equilibrium. The observed phenomena could be explained by the denser cross-linking in the dendritic hydrogels due to the shorter L-PEG segments and greater availability of cross-link functions on the periphery of the more rigid dendritic globules.

Thermal Phase Transitions of Water Adsorbed in the Hydrogels. It is known that the water absorbed in polymer systems is affected by specific interactions with the polymer chains. Because of the widespread usage, the interactions of PEG with water and the hydrated structure of PEG molecules have been studied extensively.[26] The mobility of the absorbed water in PEG hydrogels is of particular importance for their use in sustained release, tissue engineering, and other biomedical and biotechnological applications. Numerous works have studied the states of water in these systems.[27−31] Differential scanning calorimetry (DSC) is a useful technique, which is very sensitive to the thermal transitions in multiphase systems and has often been applied to investigate the different states of water in hydrogels.[32] According to the literature, there are three such states: nonfreezing (bound) water, which forms the primary hydrating shell of the hydrophilic polymer chains, freezing bound water in the secondary hydration shell, and freezing (free) water, which does not interact with the network structure. The content of the three water phases depends on the degree of swelling (or water uptake). The same dependency is also observed with the hydrogels in this study. An example with S20L network (PEG content 90 wt %) is shown in Figure 12. The DSC analyses show that endothermic peaks of water melting are not observed at water uptake below 18.5 wt %, with probably only nonfreezing water present, as previously suggested for another hydrogel system.[33] When the water uptake is above 50 wt %, there are two endothermic peaks below 0 °C, indicating that in addition to the nonfreezing water two types

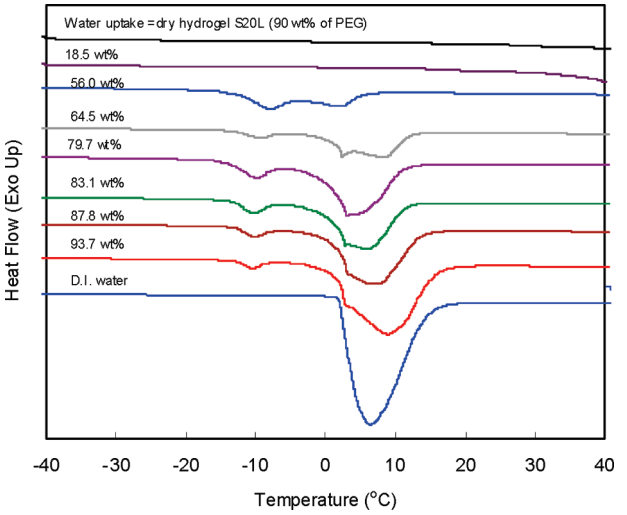

Figure 12. Representative DSC heating curves of hydrogel S20L (90 wt % of PEG) with different water uptake. Heating rate 5 °C/min.

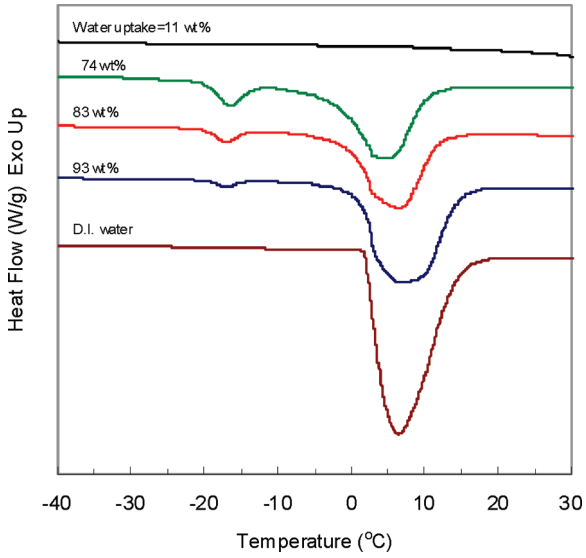

Figure 13. DSC curves of swollen L5H hydrogels (90 wt % of PEG). Heating rate 5 °C/min.

of freezing bound water appear in the system. When the water content increases, the melting endotherm at approximately −8 °C remains almost unchanged with a small shift to lower temperatures. It probably corresponds to the melting of freezing bound water in small pores, since during the swelling process their relative volume in the network would reach a "saturation" level reasonably fast. At the same time the second endotherm at ∼2 °C, which apparently is due to the freezing bound water in large pores, increases, as they expand with the increase in water uptake. When the water content attains values above 60 wt %, the melting endotherm of the free (freezing) water appears at ∼9 °C and increases with the progress of water uptake. For comparison, the heating DSC curves for hydrogel L5H with water uptakes in the range 11−93 wt % are shown in Figure 13. They show a rather similar trend with only one exception—the melting peak of the bound water is observed at −19.9 °C, significantly lower that of hydrogel S20H with similar water uptake. It is reasonable to assume that this water resides in micropores with smaller sizes, as shown by the SEM analyses of these networks. Their relative volume will decrease with

the expansion of the gel as evidenced by the decrease in their peak area (Figure 13).

The influence of the PEG content in S20L networks, which contain blocks with identical architecture, is investigated at comparable degrees of swelling (water uptake in the range of 75−90 wt %) (Figure 14). It can be seen that at PEG contents of 33 wt % the hydrogel DSC curve has endotherms corresponding to free water and freezing bound water in the large pores at temperatures similar to those of the previously discussed gels. As the PEG content increases to 50 wt % and higher, a low melting peak with increasing intensity appears around −11 °C, which could be attributed to the freezable bound water in small pores. It is also noticeable that at high PEG contents (above 80 wt %) the peaks above 0 °C converge into a relatively broad endothermic peak with a small shoulder (Figure 14). The changes in the thermal transitions characteristic of the different states of water allow us to draw the conclusion that the hydration of the hydrogels is affected not only by their chemical composition but also by the microstructure of networks.

The enthalpy of melting, calculated from the area of melting transition peak(s), could provide an estimate for the weight fractions of the water existing in the three different states via the following equation:

$$W_t = W_{nf} + W_{fb} + W_f \quad (1)$$

where W_t is the total amount of water, absorbed by the hydrogel, as measured by TGA in g H_2O per g swollen gel, W_{nf} is the nonfreezing bound water, W_{fb} is the fraction of freezable bound water, and W_f is the free water.

The areas under the DSC peaks represent the changes in enthalpy (ΔH_f) associated with melting of the different states of freezable water. In order to use the DSC data, one should assume that the water distribution is homogeneous in the swollen hydrogel, and the enthalpy of fusion of the freezable bound water is the same as that of free water. This assumption is not entirely correct since the heat of melting of freezable water depends on its degree of interaction with the surrounding polymer and is consequently not constant.[26] This melting enthalpy represents merely an upper limit that leads to a slight overestimation of the amount of nonfreezing water in the hydrogels. On the other side, the endothermic peaks of freezable bound water and free water overlap, and therefore the heat of melting per unit weight is integrated as the sum of both ($W_{fb} + W_f$). The fraction of free and freezable water in a hydrogel could be presented by the following ratio:

$$(W_{fb} + W_f)/W_{wet} = \Delta H_f/\Delta H_m \quad (2)$$

where ΔH_f is the enthalpy change, associated with the melting of freezable water per weight of a hydrogel, and ΔH_m is the enthalpy change for the melting of pure DI water. The value of ΔH_m, measured for the DI water used in this study, is 339 ± 1 J/g. The content of nonfreezing bound water (W_{nf}) is calculated by subtracting $W_{fb} + W_f$ from the total content of water absorbed by hydrogel as shown in following equation:

$$W_{nf} = W_t - (W_{fb} + W_f) = W_t - \Delta H_f/\Delta H_m \quad (3)$$

Table 8 summarizes the contents of different types of water determined by DCS at various swelling degree of hydrogels. The values for w_{total}, w_{nf}, w_{fb}, and w_f are presented as grams of H_2O per gram of dry gel before swelling. The total water content (f_{water}) in the swollen hydrogel is also included in the table and is derived as described in the Experimental Section.

The dependences of the values of $w_{fb} + w_f$ and w_{nf} on w_t for hydrogels S20L and L5H (90 wt % of PEG) are graphically

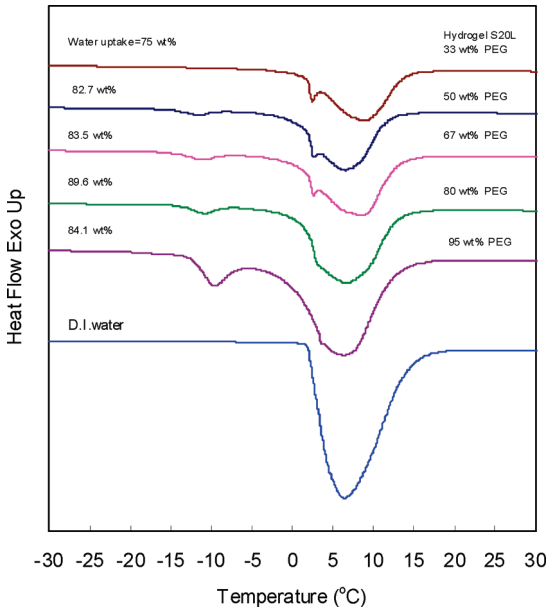

Figure 14. Influence of the PEG content on the DSC curves of S20L hydrogel series. Heating rate 5 °C/min.

Table 8. Fractions of Water in Different States Determined at Various Water Content f_{H_2O} for Hydrogels with Different Constituent Architecture (S20L and L5H)

hydrogel sample	f_{water} (%)	q (w_{wet}/w_{dry})	ΔH_f (J/g wet gel)	$\Delta H_f/\Delta H_m$	w_{total} (g H_2O/g dry gel)	$w_{fb} + w_f$ (g H_2O/g dry gel)	w_{nf} (g H_2O/g dry gel)
S20L (90 wt % PEG)	18.5	1.23	0	0	0.23	0	0.23
S20L (90 wt % PEG)	58.9	2.43	173.0	0.507	1.43	1.23	0.20
S20L (90 wt % PEG)	79.7	4.93	239.7	0.702	3.93	3.46	0.47
S20L (90 wt % PEG)	83.1	5.92	260.1	0.762	4.92	4.51	0.41
S20L (90 wt % PEG)	87.8	8.20	279.0	0.817	7.20	6.70	0.50
S20L (90 wt % PEG)	93.7	15.87	297.0	0.870	14.87	13.81	1.06
S20L (80 wt % PEG)	45.3	1.83	103.2	0.302	0.83	0.55	0.28
S20L (80 wt % PEG)	56.6	2.30	148.8	0.436	1.30	1.01	0.30
S20L (80 wt % PEG)	73.6	3.79	215.4	0.631	2.79	2.39	0.40
S20L (80 wt % PEG)	89.6	9.62	288.3	0.845	8.62	8.13	0.49
S20L (80 wt % PEG)	92.0	12.52	296.5	0.868	11.52	10.86	0.65
L5H (90 wt % PEG)	11.0	1.12	0	0	0.12	0	0.12
L5H (90 wt % PEG)	74.0	3.85	238.9	0.705	2.85	2.71	0.14
L5H (90 wt % PEG)	82.9	5.85	270.8	0.799	4.85	4.67	0.18
L5H (90 wt % PEG)	92.7	13.7	308.6	0.910	12.70	12.47	0.23

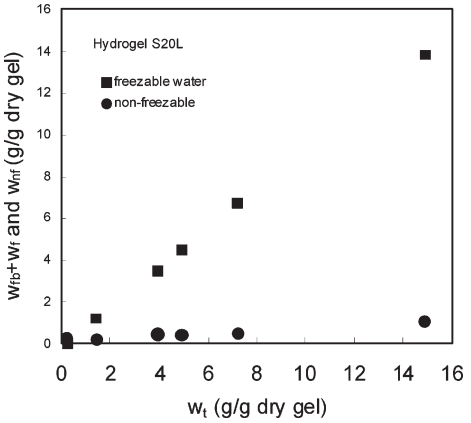

Figure 15. Dependence of $w_{fb} + w_f$ and w_{nf} on total content of water adsorbed in hydrogel S20L (90 wt % of PEG).

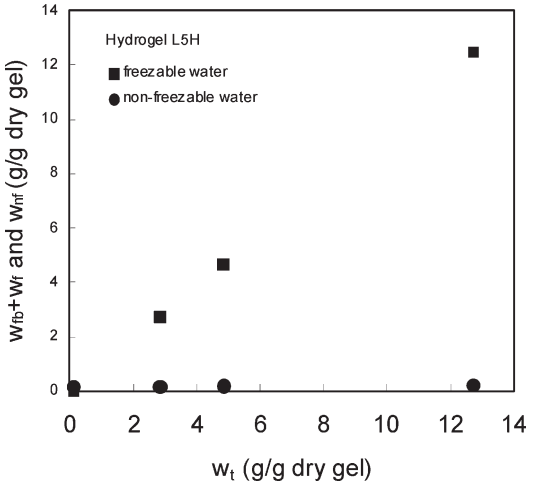

Figure 16. Dependence of $w_{fb} + w_f$ and w_{nf} on total content of water adsorbed in hydrogel L5H (90 wt % of PEG).

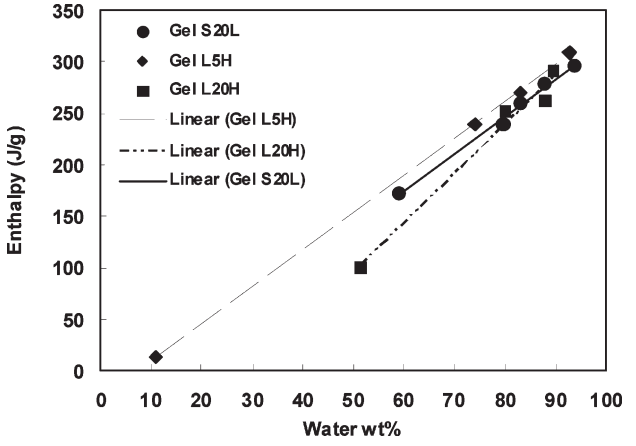

Figure 17. Enthalpy (ΔH) changes, associated with melting of freezable water in hydrogels with comparable compositions (90 wt % of PEG) as a function of the water content (W_t). DSC fitting data as follows: (◆) $\Delta H = 3.60W_t - 26.83$ ($R = 1$); (●) $\Delta H = 3.61W_t - 41.42$ ($R = 0.99$); (■) $\Delta H = 4.78W_t - 143.4$ ($R = 0.98$).

shown in Figures 15 and 16, respectively. It is seen that the amount of freezing water ($w_{fb} + w_f$) increases almost linearly with the increase in total water content, while the amount of nonfreezable is comparatively very small and remains almost constant over the whole range investigated.

The values for the enthalpy associated with melting of freezing water (ΔH_f) of several hydrogels are plotted as a function of the water uptake in Figure 17. With the increase of the water content ΔH_f increases as well. As expected, the ΔH_f values are lower than those estimated on the assumption that all water absorbed in the hydrogels behaves as freezable (free) water (i.e., lower than 339 ± 1 J/g). This is a clear indication that a certain amount of water in the hydrogels is unable to freeze. The intercepts on the *X*-axis in Figure 17 for each linear slope fitting yield the maximum amounts of nonfreezing water in the corresponding networks. Thus, the portion of nonfreezing bound water in the primary hydration shell of the hydrophilic chains in hydrogel L5H is ~7.5%, much lower than those in hydrogel S20L (11.5%) and L20H (30%). The dominant reasons for the observed differences are the length of the interjunction segments and type of PEG used in synthesis of the hydrogels. In L5H, the PEG used has the shortest chain, while L20H contains the longest. It is known that the maximum hydration number per ethylene glycol unit decreases from 3.3 through 2.4 down to 1.6 as the PEG molecular weight decreases from 70 000 through 1540 down to 400, respectively.[34] Thus, it could be assumed that the amount of bound (nonfreezing) water would follow a similar trend.

Conclusions

Amphiphilic networks can be formed by Williamson ether synthesis from linear or star PEG as the hydrophilic component and linear or hyperbranched PPCMSt as the hydrophobic one. The architecture of the macromolecules, incorporated into the hydrogels, has a pronounced effect on their cross-linking density, the porosity, and the degree of swelling. SEM micrographs show that most of the resulting networks are highly porous, and the pores within the matrixes are interconnected. The thermal phase transition behavior of the water absorbed in the hydrogels reveals that it exists in three states: freezing (free), freezing bound, and nonfreezing (bound). The results from the swelling studies, the porous structures observed in many of the hydrogels, and the mobility of the water in their interior favorably frame their potential as microfluidic devices, templates for enzyme immobilization, and suitable scaffolds for cell infiltration and growth. The presence of numerous functional groups throughout the interconnected frameworks also presents intriguing opportunities for the attachment of biologically active substances and/or cofactors for advanced biomedical and biotechnological applications, which we are currently investigating.

Acknowledgment. The authors thank Katie Bartlett and Peng Wang for their assistance in some of the preliminary experiments. Partial funding by NSF (CBET-0853454) and (CHE-0243959, REU fellowships for K.B. and P.W.) is acknowledged with thanks.

References and Notes

(1) (a) Iván, B.; Kennedy, J. P.; Mackey, P. W. In Polymeric Drugs and Drug Delivery Systems; Dunn, R. L., Ottenbrite, R. M., Eds.; ACS Symposium Series Vol. *469*; American Chemical Society: Washington, DC, 1991; pp 194−202. (b) Missirlis, D.; Tirelli, N.; Hubbell, J. A. *Langmuir* **2005**, *21*, 2605–2613. (c) Scherble, J.; Thomann, R.; Iván, B.; Mülhaupt, R. *J. Polym. Sci., Part B: Polym. Phys.* **2001**, *39*, 1429–1436.

(2) Brahim, S.; Narinesingh, D.; Guiseppi-Elie, A. *Biomacromolecules* **2003**, *4*, 497–503.

(3) (a) Iván, B.; Feldthusen, J.; Müller, A. H. E. *Macromol. Symp.* **1996**, *102*, 81–90. (b) Haigh, R.; Fullwood, N.; Rimmer, S. *Biomaterials* **2000**, *21*, 735–739. (c) Domján, A.; Erdodi, G.; Wilhelm, M.; Neidhöfer, M.; Landfester, K.; Iván, B.; Spiess, H. W. *Macromolecules* **2003**, *36*, 9107–9114.

(4) Rimmer, S.; German, M. J.; Maughan, J.; Sun, Y.; Fullwood, N.; Eddon, J.; MacNeil, S. *Biomaterials* **2005**, *26*, 2219–2230.
(5) (a) Liu, Y.-Y.; Fan, X.-D.; Wei, B.-R.; Si, Q.-F.; Chen, W.-X.; Sun, L. *Int. J. Pharm.* **2006**, *308*, 205–209. (b) Binder, W. H.; Petraru, L.; Roth, T.; Groh, P. W.; Pálfi, V.; Kéki, S.; Iván, B. *Adv. Funct. Mater.* **2007**, *17*, 1317–1326.
(6) For some leading references on amphiphilic conetworks see: (a) Erdodi, G.; Janecska, Á.; Iván, B. Novel intelligent amphiphilic conetworks. In *Wiley Polymer Networks Group Reviews*; Stokke, B. T., Elgsaeter, A., Eds.; Wiley: New York, 1999; Vol. *2*, pp 73−84. (b) Erdodi, G.; Iván, B. *Chem. Mater.* **2004**, *16*, 959–962. (c) Vamvakaki, M.; Patrickios, C. S. *Chem. Mater.* **2002**, *14*, 1630–1638. (d) Groenewolt, M.; Brezesinski, T.; Schlaad, H.; Antonietti, M.; Groh, P. W.; Iván, B. *Adv. Mater.* **2005**, *17*, 1158–1162. (e) Kali, G.; Georgiou, T. K.; Iván, B.; Patrickios, C. S.; Loizou, E.; Thomann, Y.; Tiller, J. C. *Langmuir* **2007**, *23*, 10746–10755. (f) Georgiou, T. K.; Patrickios, C. S. *Biomacromolecules* **2008**, *9*, 574–582. (g) Kafouris, D.; Gradzielski, M.; Patrickios, C. S. *Macromolecules* **2009**, *42*, 2972–2980. (h) Kali, G.; Georgiou, T. K.; Iván, B.; Patrickios, C. S. *J. Polym. Sci., Part A: Polym. Chem.* **2009**, *47*, 4289–4301.
(7) *Poly*(*ethylene glycol*). *Chemistry and Biological Applications*; Harris, J. M., Zalipsky, S., Eds.; American Chemical Society: Washington, DC, 1997.
(8) Hong, Y.; Krsko, P.; Libera, M. *Langmuir* **2004**, *20*, 11123–11126.
(9) Kang, J.; Beers, K. J. *Biomacromolecules* **2006**, *7*, 453–458.
(10) Kurian, P.; Kennedy, J. P. *J. Polym. Sci., Part A: Polym. Chem.* **2002**, *40*, 1209–1217.
(11) Erdodi, G.; Kennedy, J. P. *J. Polym. Sci., Part A: Polym. Chem.* **2005**, *43*, 4953–4964.
(12) Cima, L. G.; Lopina, S. T. *Macromolecules* **1995**, *28*, 6787–6794.
(13) Gitsov, I.; Lin, C. *Curr. Org. Chem.* **2005**, *9*, 1025–1051.
(14) (a) Gitsov, I.; Zhu, C. *Macromolecules* **2002**, *35*, 8418–8427. (b) Gitsov, I.; Lys, T.; Zhu, C. Amphiphilic Hydrogels with Highly Ordered Hydrophobic Dendritic Domains. In *Polymer Gels. Fundamentals and Applications*; Bohidar, H. B., Dubin, P., Osada, Y., Eds.; ACS Symposium Series Vol. *833*; American Chemical Society: Washington, DC, 2002; pp 218−232. (c) Gitsov, I.; Zhu, C. *J. Am. Chem. Soc.* **2003**, *125*, 11228–11234. (d) Zhu, C.; Hard, C.; Lin, C.; Gitsov, I. *J. Polym. Sci., Part A: Polym. Chem.* **2005**, *43*, 4017–4029.
(15) (a) Fréchet, J. M. J.; Hawker, C. J.; Gitsov, I.; W. Leon, J. *J. Macromol. Sci., Pure Appl. Chem.* **1996**, *A33*, 1399–1425. (b) Yates, C. R.; Hayes, W. *Eur. Polym. J.* **2004**, *40*, 1257–1281. (c) Voit, B. I.; Lederer, A. *Chem. Rev.* **2009**, *109*, 5924–5973.
(16) Gan, D.; Mueller, A.; Wooley, K. L. *J. Polym. Sci., Part A: Polym. Chem.* **2003**, *41*, 3531–3540.
(17) Gudipati, C. S.; Greenlief, C. M.; Johnson, J. A.; Prayongpan, P.; Wooley, K. L. *J. Polym. Sci., Part A: Polym. Chem.* **2004**, *42*, 6193–6208.
(18) (a) Powell, K. T.; Cheng, C.; Wooley, K. L.; Singh, A.; Urban, M. W. *J. Polym. Sci., Part A: Polym. Chem.* **2006**, *44*, 4782–4794. (b) Ohashi, R.; Bartels, J. W.; Xu, J.; Wooley, K. L.; Schaefer, J. *Adv. Funct. Mater.* **2009**, *19*, 3404–3410.
(19) Morisaku, T.; Watanabe, J.; Konno, T.; Takai, M.; Ishihara, K. *Polymer* **2008**, *49*, 4652–4657.
(20) Weimer, M. W.; Fréchet, J. M. J.; Gitsov, I. *J. Polym. Sci., Part A: Polym. Chem.* **1998**, *36*, 955–970.
(21) *Physical Properties of Polymers Handbook*; Mark, J. E., Ed.; AIP Press: Woodbury, NY, 1996; pp 177−196.
(22) (a) Flory, P. J. *Principles of Polymer Chemistry*; Cornell University Press: Ithaca, NY, 1953. (b) Ashbaugh, H. S.; Paulaitis, M. E. *Ind. Eng. Chem. Res.* **2006**, *45*, 5531−5537 and references therein.
(23) Calvino-Casilda, V.; López-Peinnado, A. J.; Vaganova, E.; Yitzchaik, S.; Pacios, I. E.; Piérola., I. F. *J. Phys. Chem. B* **2008**, *112*, 2809–2817.
(24) Zhang, X.-Z.; Yang, Y.-Y.; Chung, T.-S. *Langmuir* **2002**, *18*, 2538–2542.
(25) Song, J.; Saiz, E.; Bertozzi, C. R. *J. Am. Chem. Soc.* **2003**, *125*, 1236–1243.
(26) (a) Shibukawa, M.; Ichikawa, R.; Baba, T.; Sakamoto, R.; Saito, S.; Oguma, K. *Polymer* **2008**, *49*, 4168–4173. (b) Dormidonotova, E. E. *Macromolecules* **2002**, *35*, 987–1001. (c) Huang, L.; Nishinari, K. *J. Polym. Sci., Part B: Polym. Phys.* **2001**, *39*, 496–500. (d) Faraone, A.; Magaz, S.; Maisano, G.; Migliardo, P.; Tettamanti, E.; Villari, V. *J. Chem. Phys.* **1999**, *110*, 1801–1806. (e) Tasaki, K. *J. Am. Chem. Soc.* **1996**, *118*, 8459–8469.
(27) Quinn, F. X.; Kampff, E.; Smyth, G.; McBrierty. V. J. *Macromolecules* **1988**, *21*, 3191−3198 and references therein.
(28) Smyth, G.; Quinn, F. X.; McBrierty, V. J. *Macromolecules* **1988**, *21*, 3198–3204.
(29) Tamai, Y.; Tanaka., H.; Nakanishi, K. *Macromolecules* **1996**, *29*, 6750–6760.
(30) McConville, P.; Pope., J. M. *Polymer* **2001**, *42*, 3559–3568.
(31) Baba, T.; Sakamoto, R.; Shibukawa, M.; Oguma, K. *J. Chromatogr., A* **2004**, *1040*, 45–51.
(32) (a) Hatakeyama, T.; Quinn, F. X. *Thermal Analysis: Fundamentals and Applications to Polymer Science*; Wiley: Chichester, 1997. (b) Bouwstra, J. A.; Salomons-de Vries, M. A.; van Miltenburg, J. C. *Thermochim. Acta* **1995**, *248*, 319–327. (c) Shibukawa, M.; Ohta, N.; Onda, N. *Bull. Chem. Soc. Jpn.* **1990**, *63*, 3490–3494.
(33) Qu, X.; Wirsén, A.; Albertsson, A.-C. *Polymer* **2000**, *41*, 4589–4598.
(34) Huang, L.; Nishinari, K. *J. Polym. Sci., Part B: Polym. Phys.* **2001**, *39*, 496–506.